Asian Journal of Physics
Vol. 32, Nos 5-8 (2023) 291-302
Available on: www.asianjournalofphysics.com

ap

Theoretical study of slanted holographic gratings for application in sensing

Graceson Antony[1,2], Dervil Cody[1,2], and Izabela Naydenova[1]

[1]*Centre for Industrial and Engineering Optics, FOCAS Research Institute, Technological University Dublin, Camden Row, D08 CKP1 Dublin 8*

[2]*School of Physics, Clinical and Optometric Sciences, Technological University Dublin, Central Quad, Grangegorman lower, D07 ADY7, Dublin, Ireland*

Dedicated to Prof John Sheridan

Functionalized holographic gratings present a promising approach to the development of optical sensors. Volume phase transmission or reflection holographic gratings have been explored for the detection of chemical, biochemical, and biomedical analytes, as well as environmental parameters such as humidity, temperature, and pressure. Volume phase holographic gratings are characterized by a strong dependence of their diffraction efficiency on the angle of incidence of the probe beam. Maximum diffraction efficiency is observed at the Bragg angle; any detuning from the Bragg angle can cause a significant change in the efficiency of the gratings. The angular detuning is typically a result of the change in the average refractive index and/or the thickness of the layer in which the grating is recorded, both changes happening in the presence of the target analyte. In this work, we theoretically compare the sensitivity of unslanted and slanted volume transmission holographic gratings to angular detuning caused by the presence of the analyte. We demonstrate that slanted gratings are more sensitive to Bragg angle detuning caused by the target analyte. We also demonstrate that in the case of slanted gratings, the sensitivity depends on the choice of the probe beam, which in this case is incident at different angles to the grating and this must be considered when the sensor device is designed.

Keywords: Holographic sensors, Volume phase transmission holograms, Slanted holographic gratings, Diffraction gratings.

1 Introduction

Holographic sensors are photonic structures that are inscribed in functionalized photosensitive layers that can change their diffractive properties under exposure to the target analyte [1-2]. The typical changes observed due to the presence of the analyte are: change in the diffraction efficiency of the hologram and/or change in the spectral characteristics of the diffracted light. Most of the sensors reported in the literature are based on reflection holograms [1-3]. This configuration offers a colorimetric response which can be registered electronically or visually in the form of indicator. The second visual option is particularly useful when a low cost, easy to interpret indicator is developed. Another configuration utilizes volume phase transmission holographic gratings (VPTHG). They require electronic read-out and are easier to mass manufacture. Because of their versatile properties, holographic sensors are a sensor platform that can find applications in different fields as shown in (Fig 1). Research efforts in holographic sensor development [4-14] are focused on three main areas (Fig 2).

Corresponding author
e mail: izabela.naydenova@TUDublin.ie (Izabela Naydenova)

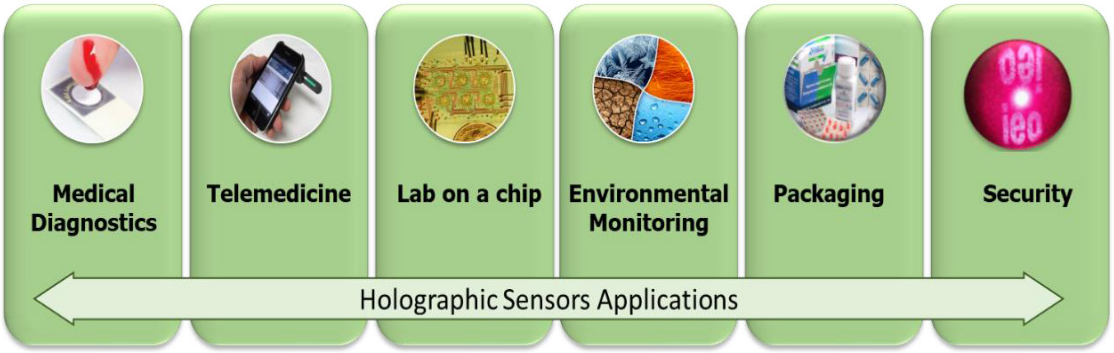

Fig 1. Range of applications for holographic sensors.

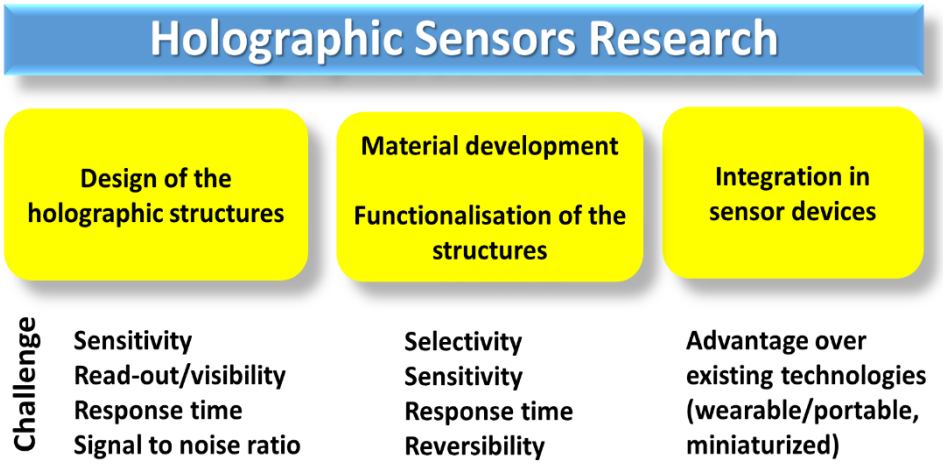

Fig 2. Three main areas of holographic sensors research and the challenges to be addressed by each area.

Sensitivity of the sensor is one of the key characteristics that needs further improvement. Previous studies analyzed the factors determining the sensitivity of holographic unslanted gratings [15]. The theoretical modelling identified that the probe beam wavelength, the grating thickness and spatial frequency are key factors of the holographic structure determining the sensitivity. In addition, it is expected that introducing a slant angle between the grating's planes and the surface of the layer can increase the grating sensitivity due to the expected higher Bragg angle detuning. This article investigates quantitatively, through numerical simulations, the effects of introducing a slant angle on the response of volume transmission holographic gratings to changes in the layer's thickness and/or average refractive index caused by the presence of the target analyte. To simplify the analysis and better distinguish the difference between slanted and unslanted grating due to their different geometric characteristics, this study assumes no change in the refractive index modulation of the grating.

2 Background

Volume phase transmission holographic gratings are recorded in the photosensitive layer in the form of periodic fringes of spatially varying refractive index. Depending on the geometry of recording two types of gratings can be recorded: unslanted, when the two recording beams have same incident angles (Fig 3(a)) and slanted when the two recording beams are incident at different angles (Fig 3(b)).

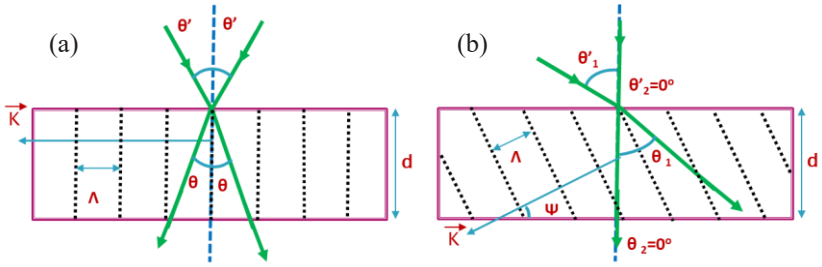

Fig 3. Holographic grating structures with identical spatial frequency at different slant angles: (a) unslanted, (b) slanted grating where one of the beams is normal to the surface of the later.

The slant angle (Ψ) is determined by the angles of incidence θ_1 and θ_2 inside the layer as shown in Fig 3(b):

$$\Psi = \frac{\theta_1 + \theta_2}{2} \tag{1}$$

The diffraction efficiency of a VPTHG is described with high accuracy by Kogelnik's Coupled Wave Theory (KCWT)[16]. The KCWT assumes that in addition to the zero-order beam, there is only one diffraction order propagating through the layer; the amplitudes of the beams change slowly as they propagate in the medium, thus the second derivatives of their amplitudes in space are zero; the diffraction from the boundaries of the layer is ignored. The KCWT provides an analytical expression for the diffraction efficiency (η) of VPTHGs, given by Eq (2):

$$\eta = \frac{\sin^2 (\nu^2 + \xi^2)^{1/2}}{\left(1 + \frac{\xi^2}{\nu^2}\right)^{1/2}} \tag{2}$$

$$\text{where } \nu = \frac{\pi n_1 d}{\lambda_{probe}.(C_R.C_S)} \tag{3}$$

is the phase difference accumulated between the probe and the diffracted beam of wavelength, λ_{probe} as they pass through the gratings with thickness d, period Λ and refractive index modulation n_1. C_R and C_S are oblique factors and are described by Eqs (4) and (5) as follows:

$$C_R = \cos \theta_B \tag{4}$$

$$C_S = \cos \theta_B + \frac{\lambda}{n_{avg}.\Lambda} \sin \Psi \tag{5}$$

where θ_B is the Bragg angle, the angle between the probe beam inside the medium and the grating planes, at which maximum diffraction efficiency is observed and is given by:

$$\theta_B = \frac{\theta_1 - \theta_2}{2} \tag{6}$$

For an unslanted grating, $\Psi = 0$, and $\nu = \frac{\pi . n_1 . d}{\lambda_{probe}.\cos \theta_B}$ (7)

The angular detuning parameter ξ is given by Eq (8):

$$\xi = \frac{\Delta\theta_p . K . d . \sin(\Psi - \theta)}{2 C_S} \tag{8}$$

where $\Delta\theta_p$ is the detuning from the Bragg angle, and K is the grating vector.

When the layer is exposed to the analyte, both the thickness of the layer and the average refractive index could change, thus causing Bragg angle detuning (Eq 8), (Fig 4).

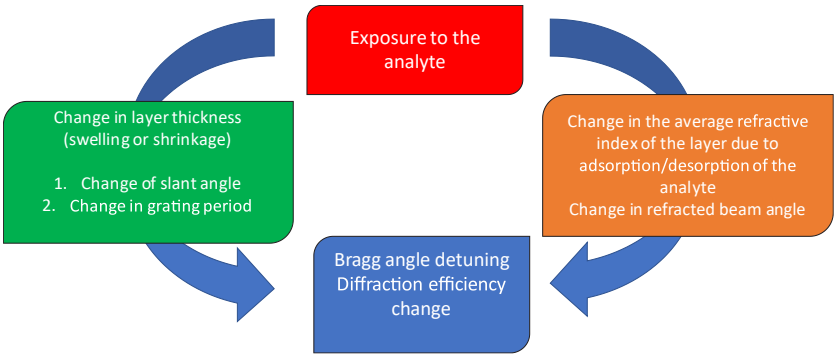

Fig 4. Illustration of the links between changes in the layer thickness and average refractive index and the resultant Bragg angle detuning.

The expected effect of the Bragg angle detuning on the change of the diffraction efficiency of the grating due to analyte exposure is illustrated in Fig 5. It is clearly seen that for the same absolute change in the maximum diffraction efficiency ($\Delta\eta_2$) due to the target analyte, the measured change in the diffraction efficiency of the grating ($\Delta\eta_1$) can be significantly larger due to the additional change in Bragg angle and a shift in the Bragg curve. In this case the probe beam is incident at constant angle θ_1', while the new Bragg angle is θ_2'.

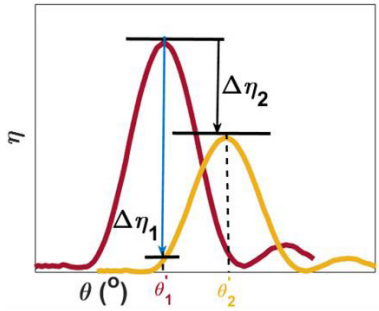

Fig 5. Angular selectivity curves for a volume phase transmission grating which has undergone a Bragg angle shift due to analyte exposure. $\Delta\eta_1$ indicates the diffraction efficiency change that will be measured by a fixed probe beam incident at the original Bragg angle θ_1' after a Bragg angle shift has taken place; $\Delta\eta_2$ indicates the diffraction efficiency change that will be measured by a probe beam that is incident on the grating at the new Bragg angle, θ_2'.

3 Methodology

In the present work, the theoretical simulations assume that the probe beam is a collimated monochromatic laser beam. For practical applications, this will need to be further expanded to cases where the light source is a low cost source emitting at a broader wavelength range, for example an LED. For the sake of simplicity and to understand better the different factors influencing the diffraction efficiency change, we consider that the refractive index modulation in the grating remains constant, and there is Bragg angle shift/detuning due to the change in thickness and change in the average refractive index of the layer.

In the following sections, we describe the methodology of calculation of the Bragg angle detuning due to thickness change (through the change in the slant angle and grating period) and due to average refractive index change (through the change in the refracted beam direction), as explained in Fig 4. First, we explore the relationships between the grating's key parameters and the change in layer thickness and in average refractive index.

3.1 Slant angle

The change of slant angle ($\Delta\psi$) due to change of the layer thickness can be expressed with the help of Eq (9):

$$\Delta\psi = \Psi_1 - \cot^{-1}\left[\left(\frac{1+\Delta d}{d}\right)\cot\Psi_0\right] \tag{9}$$

Here, Ψ_1 and Ψ_0 are the final and initial slant angles, respectively.

The slant angle change depends only on dimensional change of the grating on exposure to the analyte, i.e. on the dimensional change Δd, the initial layer thickness d and the initial slant angle. The slant angle shift ($\Delta\psi$) along with the probe beam shift determines the overall detuning from the Bragg angle inside the hologram, see Eq (10).

$$\Delta\theta_B = \Delta\Psi - \Delta\theta_2 \text{ or } \Delta\theta_B = \Delta\theta_1 - \Delta\Psi \tag{10}$$

Here, $\Delta\theta_B$ is the Bragg angle shift inside the medium, $\Delta\theta_1$ and $\Delta\theta_2$ are the respective angular shift in the probe beams.

In a slanted grating there are two possible probe beam directions that are asymmetric with respect to the normal of the grating. Each of the two probe beams, incident at a different angle on the grating, can experience different Bragg angle detuning after exposure of the grating to the analyte, (Eq 10).

3.2 Grating period

The grating period (Λ) is determined by the recording beams wavelength and their inter-beam angle at the recording stage. It can also be expressed in terms of the Bragg angle θ_B, at which for specific probe beam wavelength λ_{probe}, maximum diffraction efficiency is observed as in Eq (11):

$$\Lambda = \frac{\lambda_{probe}}{2n_{avg}\sin(\theta_B)} \tag{11}$$

As a result of the layer thickness change, the grating period will also change as previously described in the study [11].

3.3 Change in probe beam angle inside the layer due to change in average refractive index

As the probe beam enters the layer it is refracted. Any change in the average refractive index will lead to a change in the refracted beam direction, thus causing a detuning from the Bragg angle for the fixed probe beam wavelength.

The value of $\Delta\theta_{probe}$ (depending on the direction of probing, either $\Delta\theta_1$ or $\Delta\theta_2$) is determined by the average refractive index change and can be calculated using Snell's law with the help of Eq (12):

$$\Delta\theta_{probe} = \frac{\Delta n_{avg}\,\sin\theta'_{probe}}{n_{avg}\sqrt{n_{avg}^2 - \sin^2\theta'_{probe}}} \tag{12}$$

where θ'_{Probe} is the incident angle of the probe beam in air.

3.4 Gratings geometries

Two different grating configurations were examined (Fig 3). The thickness of the layers was 60 μm. The spatial frequency of the examined gratings was fixed at 1200 line-pairs/mm. This spatial frequency was selected to ensure that the gratings are operating as VPTHG for which the KCWT is applicable. The sensitivity in terms of Bragg angle detuning and resulting diffraction efficiency change was compared for unslanted and slanted grating with one of the two probe beams: (1) normal to the surface of the layer; (2) incident at an angle θ_1', (Fig 3(b)).

The slant angle for the slanted gratings was 12° degrees. The slant angle was selected to remain constant in this investigation. The sensitivity of the grating for a range of different slant angles will be

reported elsewhere. The physical changes in the layer which occur as a result of analyte exposure were selected to be within 10% of the original value of the thickness (60 μm) and the average refractive index (1.5). Thus, the thickness was varied in the range of ± 6 μm and the average refractive index was changed within ± 0.02. The initial diffraction efficiency of the grating was selected to be 50%. This was done to ensure a linear regime of operation for the range of changes studied.

A MATLAB programme was created to calculate numerically the Bragg angle detuning $\Delta\theta_B$ for each pair of thickness and average refractive index within the range of studied values. The resulting change in diffraction efficiency η (Eq 2) was then determined by running numerical simulations to calculate v (Eq 3) and ξ (Eq 8) for each possible combination of n_{avg} and d.

4 Results and discussion

4.1 Unslanted grating

Figure 6 shows the calculated Bragg angle detuning in an unslanted grating for the studied thickness and average refractive index ranges. Figure 6(a) shows the map of angular Bragg detuning parameter $\Delta\theta_B$. It can be observed that the maximum absolute values for $\Delta\theta_B$ are in the order of ±0.1° for all possible combinations of change in thickness and average refractive index. Even relatively small detuning such as this can have a significant contribution; for example for a 1200 line-pairs/mm grating with a thickness of 60 μm, the FWHM of the Bragg selectivity curve is in the order of 0.8°, and so a ± 0.1° change may be significant. Figure 6(b) shows $\Delta\theta_B$ versus the change in layer thickness due to analyte exposure for a number of scenarios: where there is no change in the average refractive index of the grating, and where there is a maximum average refractive index change (both in the positive (blue) or negative (red) directions). It is worth noticing that even if there is a thickness change in this case, no Bragg detuning is observed in the absence of a change in the average refractive index (orange line). Figure 6(c) shows that the angular Bragg detuning in this case is fully symmetrical with respect to the sign of the average refractive index change as would be expected. As expected (from Eq 12), the maximum positive $\Delta\theta_B$ is found at the lowest value for n_{avg} while maximum negative $\Delta\theta_B$ is found at highest n_{avg} value. Moreover, Fig 6(c) further confirms that the value of Δd has no effect on the extent of Bragg detuning for unslanted gratings.

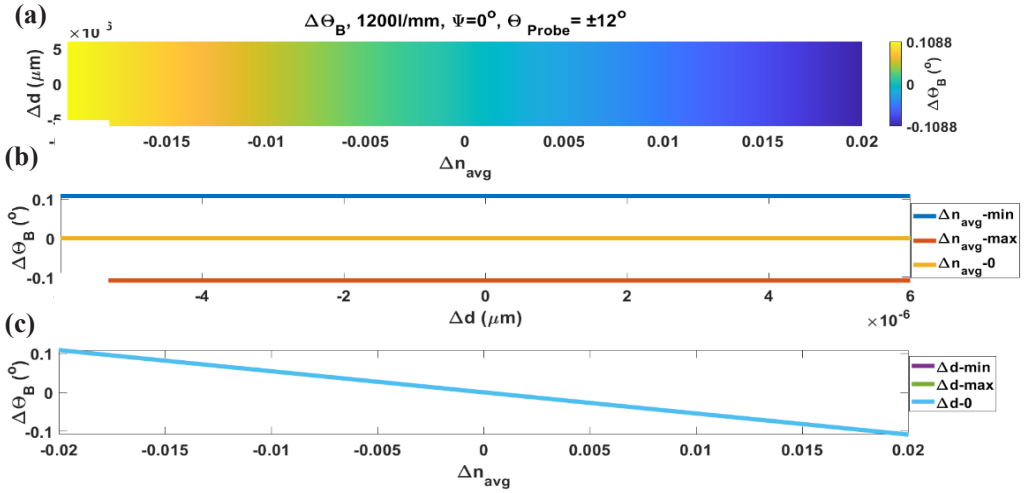

Fig 6. Bragg angle detuning $\Delta\theta_B$ for an unslanted grating at a spatial frequency of 1200 lines/mm. (a) $\Delta\theta_B$ map for all combinations of Δn_{avg} and Δd; (b) $\Delta\theta_B$ versus Δd at three different Δn_{avg} values; (c) $\Delta\theta_B$ versus Δn_{avg} at three different Δd values.

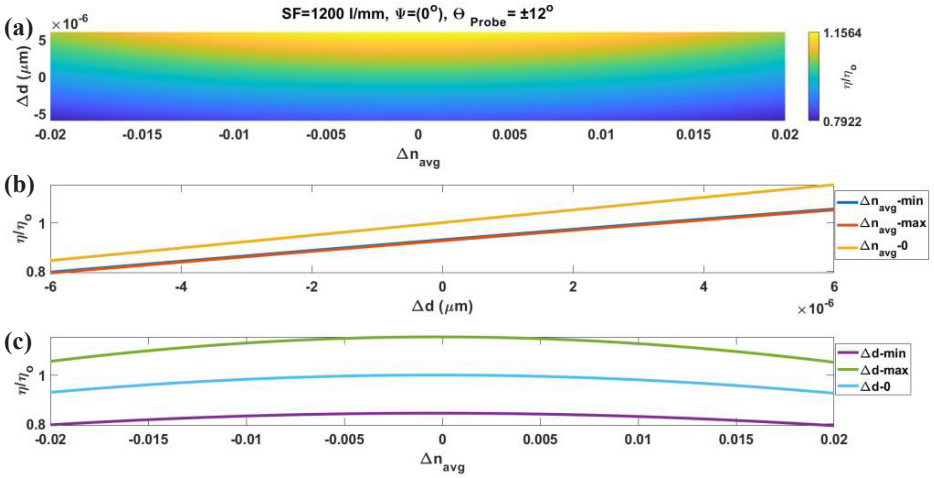

Fig 7. (a) A colour map of the expected change in diffraction efficiency for an unslanted grating for all possible combinations of the Δn_{avg} and Δd; (b) diffraction efficiency versus grating thickness for three values of the Δn_{avg}; (c) diffraction efficiency versus Δn_{avg} for three values of grating thickness.

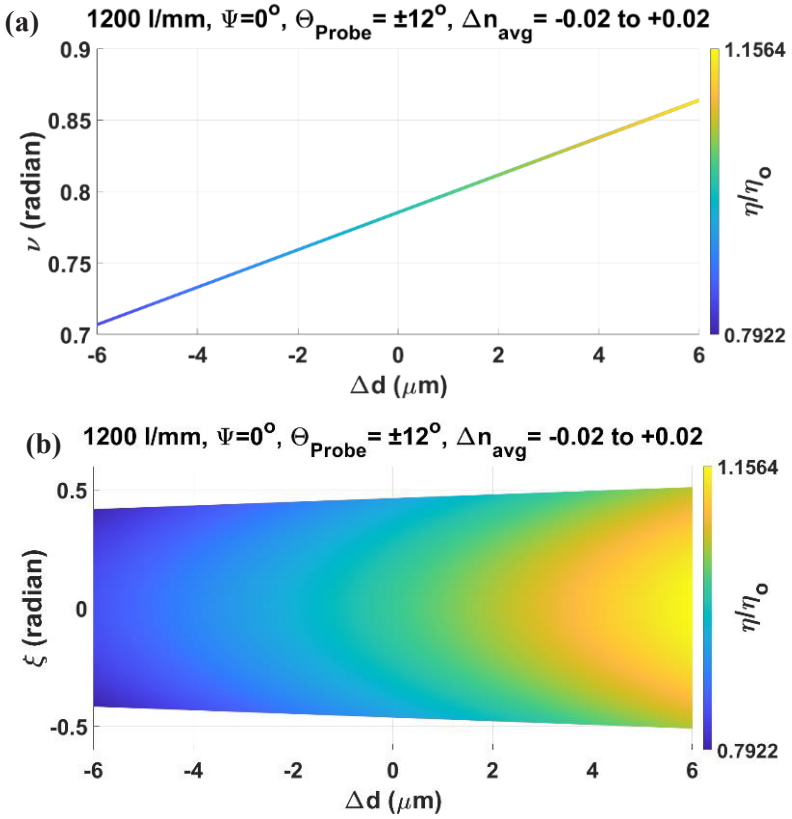

Fig 8. Maps of the normalized diffraction efficiency of an unslanted grating for varying layer thickness and average refractive index. (a) Corresponding dependence of ν on thickness change; (b) corresponding dependence of ξ on thickness change.

In the next step, the values for $\Delta\theta_B$ were used to calculate the Bragg angle detuning parameter ξ (Eq 8) and the phase parameter ν (Eq 3). A colour map of the expected change in diffraction efficiency is shown in Fig 7(a) for all possible combinations of the Δn_{avg} and Δd. It can be observed that the maximum increase (approximately 15.6%) of the diffraction efficiency ratio occurs at the maximum positive Δd (grating thickness increased from 60 to 66 μm) and at $\Delta n_{avg} = 0$ (Fig 7(b)), while the maximum diffraction efficiency ratio decrease (approximately 21%) is observed at the maximum studied negative Δd (grating thickness reduced from 60 to 54 μm) and for maximum studied absolute value of Δn_{avg}. According to the simulations, the sign of the Δn_{avg} has no effect on the diffraction efficiency change at specific Δd (Fig 7(b)). Figure 7(c) shows the dependence of the diffraction efficiency change on the Δn_{avg} for three values of Δd. It is seen that the impact of a 10% change in thickness on the observed diffraction change is significantly higher than that of a 10% change in Δn_{avg}.

To fully understand their contributions to the overall diffraction efficiency, the values of the Bragg angle detuning parameter ξ (Eq 8) and the phase parameter ν (Eq 3) are shown separately in Fig 8.

From these two maps it is seen that the variation of average refractive index has little impact on ν, the spread of values at a particular Δd is small compared to the spread observed in ξ. An asymmetry in the dependence of ξ on grating thickness is also observed in Fig 8(b).

4.2 Introducing a slant angle

Next we examine the case where a slant angle of 12° is introduced. Two different probe beam configurations are considered: (1) the probe beam is normal to the grating surface (θ_{probe}= 0°) and (2) the probe beam is incident at 24° (i.e. $\theta_{probe} = \theta_B + \Psi$). Examination of the two 2D maps of the Bragg angular detuning for the slanted grating (Figs 9(a & b)) shows that the value of maximum $\Delta\theta_B$ has increased by an order of magnitude in comparison to the unslanted grating (Fig 6(a)); that is, from the 0.1° observed in an unslanted grating to more than 1° in a slanted grating.

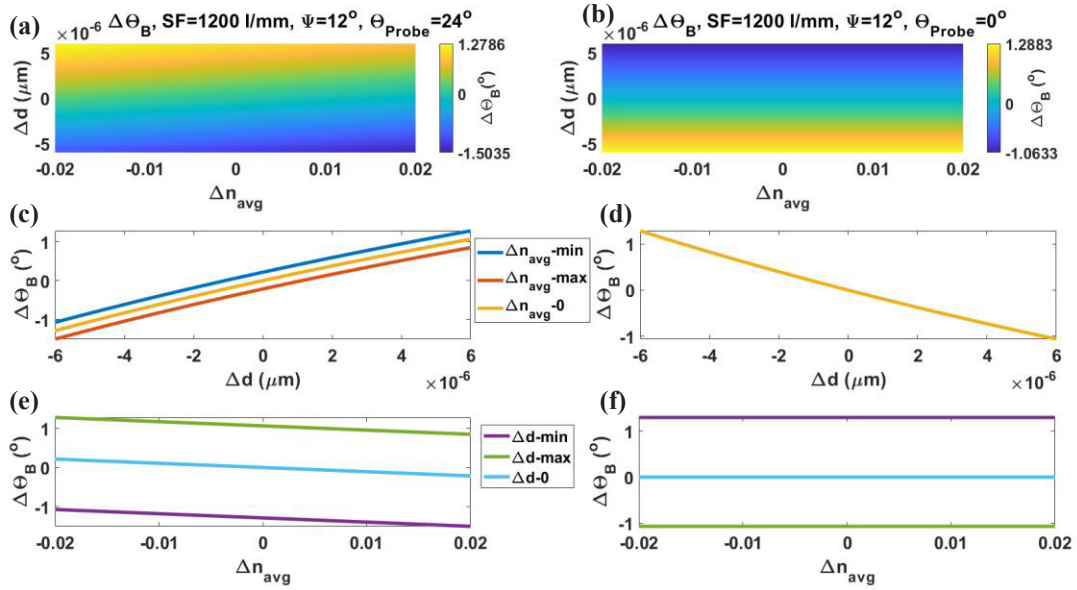

Fig 9. $\Delta\theta_B$ for a slanted grating with a spatial frequency of 1200 lines/mm for two different probe beam configurations. (a) $\Delta\theta_B$ distribution for all combinations of Δn_{avg} and Δd at $\theta_{probe} = \theta_B + \Psi$. (b) $\Delta\theta_B$ distribution for all combinations of Δn_{avg} and Δd at $\theta_{probe} = 0°$. (c) $\Delta\theta_B$ versus Δd at different Δn_{avg} conditions when $\theta_{probe} = \theta_B + \Psi$. (d) $\Delta\theta_B$ versus Δd at different Δn_{avg} conditions when $\theta_{probe} = 0°$. (e) $\Delta\theta_B$ versus Δn_{avg} values at different Δd conditions when $\theta_{probe} = \theta_B + \Psi$. (*f*) $\Delta\theta_B$ versus Δn_{avg} values at different Δd conditions when θ_{probe}= 0°.

This result is independent of the angle of the probe beam used. As previously mentioned, the FWHM of a 1200 lines/mm and 60 μm thick grating is approximately 0.8°. A 1° change in the Bragg angle due to analyte-induced changes in grating thickness and average refractive index is thus highly significant and, as shown earlier in Fig 5, can be exploited to maximize the sensitivity of VPTHG-based sensors.

Another interesting observation is the highly asymmetric dependence of the Bragg angular detuning for the probe beam incident at 24° (Figs 9(c & d)), and the highly symmetric response for the probe beam at normal incidence (Figs 9 (d & f)). The use of a probe beam that is incident normal to the layer also removes any sensitivity to analyte-induced changes in the average refractive index of the grating. This is potentially a very useful result. In slanted gratings, change in thickness due to layer swelling or shrinkage plays a significant role in the response of the grating to the presence of the analyte. It is worth noting that if one aims at evaluating separately the two effects – thickness change and average refractive index change - a measurement system with two probe beams incident from both directions could be used for analysis, to allow for separation of the influence of thickness change and average refractive index change on the overall sensor response to an analyte.

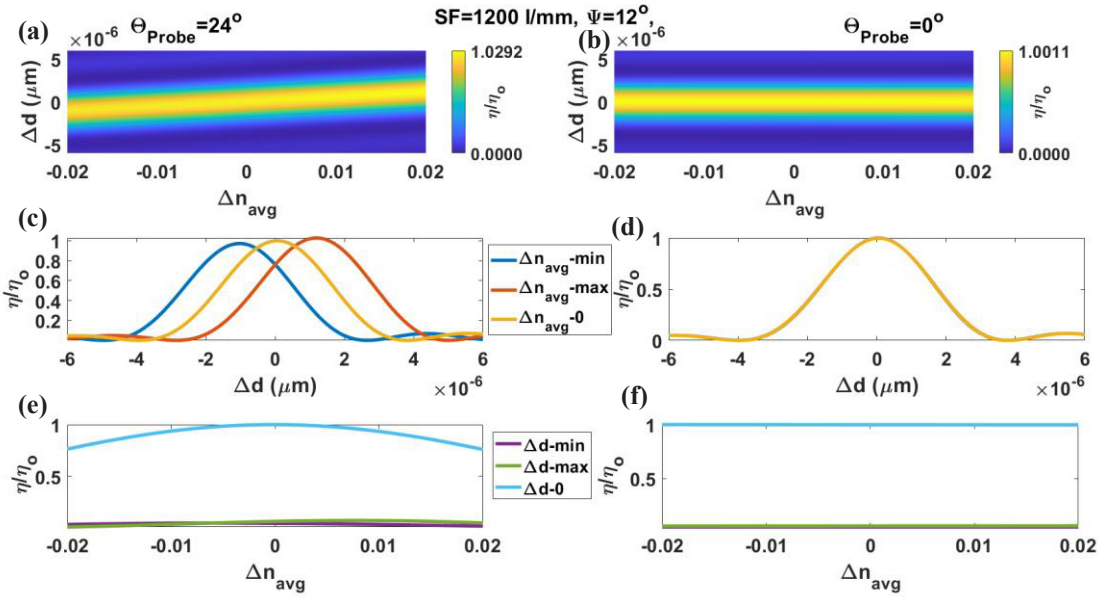

Fig 10. Map of the diffraction efficiency change of slanted grating as d and n_{avg} change; (a) diffraction efficiency change distribution for all combinations of Δn_{avg} and Δd at $\theta_{probe} = \theta_B + \Psi$. (b) diffraction efficiency change distribution for all combinations of Δn_{avg} and Δd at $\theta_{probe} = 0^o$. (c) diffraction efficiency change versus Δd at different Δn_{avg} conditions when $\theta_{probe} = \theta_B + \Psi$. (d) diffraction efficiency change versus Δd at different Δn_{avg} conditions when $\theta_{probe} = 0°$. (e) diffraction efficiency change versus Δn_{avg} values at different Δd conditions when $\theta_{probe} = \theta_B + \Psi$. (d) diffraction efficiency change versus Δn_{avg} values at different Δd conditions $\theta_{probe} = 0°$.

Figure 10 illustrates the expected change in diffraction efficiency for the slanted grating for all possible combinations of the Δn_{ave} and Δd, and for both probe beam configurations. As expected, the observed changes in diffraction efficiency are significantly larger for the slanted grating in comparison to the unslanted grating scenario (Fig 7), indicating improved sensitivity for slanted grating-based sensor configurations. The diffraction efficiency is seen to drop to zero for specific combinations of changes in thickness and average refractive index. For example, the diffraction efficiency goes to zero at around ± 4 μm change in thickness for the slanted grating at normal incidence (Fig 10 (d)).

For the probe beam incident on the grating at 24°, the analyte-induced change in the grating's average refractive index is seen to influence the change in diffraction efficiency (Fig 10(c)); an asymmetry

in the response of the grating to changes in grating thickness is also observed. In Fig 10(c), it can be clearly seen that for the maximum studied analyte-induced refractive index changes (both positive and negative), there are corresponding thickness changes that, if occurring concurrently, will act to negate any measurable change in diffraction efficiency, thus preventing a detectable sensor response to the analyte. This emphasizes the importance of the careful theoretical design of the sensor. The contribution of average refractive index alone to the diffraction efficiency change at 24° probe angle can be found in Fig 10 (e, blue line); the response of the diffraction efficiency drop is symmetrical with respect to the absolute change in average refractive index. A large diffraction efficiency drop is observed for the maximum studied absolute change in thickness over the whole range of Δn_{avg} (Fig 10 (e)).

As was seen earlier for the Bragg detuning studies, at normal probe beam incidence, the change in diffraction efficiency of the slanted grating is due only to the change in the grating thickness, and does not depend on the average refractive index change (Fig 10 (d) and (f)). This is a beneficial result that can be exploited for material characterization and sensor development purposes.

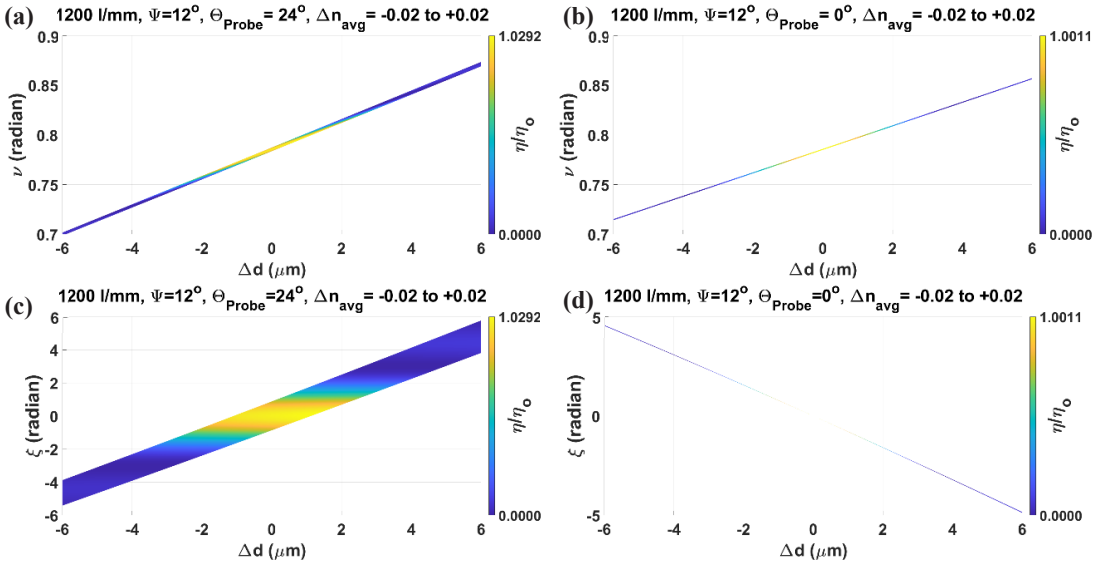

Fig 11. Maps of normalized diffraction efficiency of a slanted grating for varying layer thickness and average refractive index. (a) corresponding dependence of ν on thickness change when probing at 24°; (b) corresponding dependence of ν on thickness change when probing at 0°. (c) corresponding dependence of ξ on thickness change when probing at 24°); (d) corresponding dependence of ξ on thickness change when probing at 0°.

Figure 11(a, b) shows that over the studied range of Δd, only a slight difference in magnitudes of ν has been observed for both incident beams. Figure 11(a, b) also shows that, for the slanted structure, any absolute change in Δd will result in a drop in diffraction efficiency. This is different to what was observed for the unslanted structure (Fig 8 (a)), where the relationship between diffraction efficiency and thickness change was seen to be linear (i.e., as the layer swells, diffraction efficiency increases). In Fig 11(c,d), as expected a higher magnitude of ξ is observed (for both probe beams) for the slanted grating structure, in comparison to that shown previously for the unslanted grating structure (Fig 8(b)). It can also be seen that the direction of change of ξ varies depending on the angle of incidence of the probe beam. The average refractive index change has no impact when probing at 0°, and so a larger spread in ξ values at a particular Δd is observed for the case where the probe beam is incident on the grating at 24° (Fig 11(c,d)).

5 Conclusions

The objective of this study was to compare theoretically the sensitivity of unslanted and slanted volume transmission holographic gratings to angular detuning, which is caused by the presence of a target analyte. The angular detuning and subsequent change in grating diffraction efficiency occur due to analyte-induced simultaneous changes in grating thickness and average refractive index; through careful design of the holographic grating structure, this angular detuning can be utilised to yield significant improvements in optical sensor performance.

The extent of angular detuning and the resultant effect on grating diffraction efficiency was calculated for both unslanted and slanted gratings. An order of magnitude increase in the amount of Bragg angle detuning was achieved by the introduction of a 12° slant angle. Angular detuning of more than 1° was estimated for a 1200 lines/mm and 60 μm slanted grating for a 10% change in the grating's thickness and average refractive index; this is a highly significant amount of detuning in the context of a grating with an angular selectivity curve FWHM of 0.8°, and demonstrates the potential of slanted gratings for highly sensitive sensing applications.

The influence of the orientation of the probe beam on the extent of angular detuning and diffraction efficiency change were also investigated. It was observed that probing of slanted gratings at normal incidence completely mitigates the effects of angular detuning due to changes in the grating's average refractive index; in contrast, probing at another angle (24°) introduces a highly asymmetric response. This important result can be exploited to allow for separate analysis of the changes in grating thickness and average refractive index which occur simultaneously in many VPTHG-based sensors during target analyte exposure. Future studies will explore in detail the influence of slant angle on the extent of grating angular detuning, as well as the influence of probe beam wavelength.

References

1. Naydenova I, Optical Holography: Materials, Theory and Applications; Blanche P A (Ed), (Elsevier), 2019.
2. Yetisen A K, Naydenova I, Vasconcellos F D C, Blyth F, Lowe C R, Holographic Sensors: Three-Dimensional Analyte-Sensitive Nanostructures and Their Applications, *Chem Rev*, 114(2014)10654–10696.
3. Zawadzka M, Mikulchyk T, Cody D, Martin S, Yetisen A K, Martinez-Hurtado J L, Butt H, Mihaylova E, Awala H, Mintova S, Yun S Y, Naydenova I, Photonic Materials for Holographic Sensing, In Photonic Materials for Sensing, Biosensing and Display Devices, (Springer), 2016, pp 315–359.
4. Ahmed I, Elsherif M, Park S, Yetisen A K, Butt H, Nanostructured Photonic Hydrogels for Real-Time Alcohol Detection, *ACS Appl Nano Mater*, 5(2022)7744–7753.
5. Branigan E, Martin S, Sheehan M, Murphy K, Modelling Spherical Aberration Detection in an Analog Holographic Wavefront Sensor, In Adaptive Optics and Applications; (Optica Publishing Group), 2022; paper OF2B-4.
6. Davies S, Hu Y, Blyth J, Jiang N, Yetisen A K, Reusable Dual-Photopolymerized Holographic Glucose Sensors. *Adv Funct Mater*, 33(2023)2214197; doi.org/10.1002/adfm.20221419.
7. Gul S E, Holographic Sensors for the Detection of Liquid Phase Analytes, Doctoral Thesis, Technological University Dublin. 2019, doi. 10.21427/14kz-5r43.
8. Irfan M, Martin S, Naydenova I, Temperature-Sensitive Holograms with Switchable Memory, *Adv Photonics Res*, 2(2021)2100062; doi.org/10.1002/adpr.202100062.
9. Mikulchyk T, Development of holographic sensors for monitoring relative humidity and temperature, Doctoral Thesis. Technological University, Dublin. 2016; doi:10.21427/D7HS3X
10. Mora M P, Ramirez M G, Brocal F, Ortuño M, Beléndez A, Pascual I, Influence of Tert-Butylthiol and Tetrahydrofuran on the Holographic Characteristics of a Polymer Dispersed Liquid Crystal: A Research Line toward a Specific Sensor for Natural Gas and Liquefied Petroleum Gas, *Polymers*, 11(2019)254; doi.org/10.3390/polym11020254.
11. O'Neill F T, Lawrence J R Sheridan J T, Thickness Variation of Self-Processing Acrylamide-Based Photopolymer and Reflection Holography, *Opt Eng*, 40(2001)533–539.

12. Sartain F K, Yang X, Lowe C R, Holographic Lactate Sensor, *Anal Chem*, 78(2006)5664–5670.
13. Tan E V, Lowe C R, Holographic Enzyme Inhibition Assays for Drug Discovery, *Anal Chem*, , 81(2009)7579–7589.
14. Yu D, Liu H, Mao D, Geng Y, Wang W, Sun L, Lv J, Holographic Humidity Response of Slanted Gratings in Moisture-Absorbing Acrylamide Photopolymer, *Appl Opt*, 54(2015)6804–6812.
15. Cody D, Naydenova I, Theoretical Modeling and Design of Photonic Structures in Zeolite Nanocomposites for Gas Sensing. Part II: Volume Gratings, *J Opt Soc Am A*, 35 (2018)12–19.
16. Kogelnik H, Coupled Wave Theory for Thick Hologram Gratings, In Landmark Papers On Photorefractive Nonlinear Optics; (World Scientific), 1995, pp 133–171.

[*Received*: 05.07.2023; *accepted*: 25.08.2023]

Mr Graceson Antony is a doctoral research candidate at the Centre for Industrial and Engineering Optics, Technological University Dublin. Graceson Antony received his M Sc in Photonics from Cochin University of Science and Technology in June 2016. His Current research interests are primarily in developing holographic sensors for gas-sensing applications. e-mail: D17128764@mytudublin.ie

Dr Dervil Cody is a Lecturer in Physics at Technological University Dublin, and a Principal Investigator in the Centre for Industrial and Engineering Optics. Dr Cody received her Ph D in Holography from TU Dublin in February 2015. Dr Cody's current research interests are primarily in the development of optical materials and sensors for medical quality assurance applications. She is a professional member of the Irish Assocation of Physicists in Medicine. A full list of Dr. Cody's research publications can be found here: https://orcid.org/0000-0002-8921-0201. e-mail: dervil.cody@tudublin.ie

Prof Izabela Naydenova is the Head of Physics and Clinical Measurement Science at Technological University Dublin, and a Principal Investigator in the Centre for Industrial and Engineering Optics. She received her PhD in Physics from the Bulgarian Academy of Sciences in 2000. After a postdoctoral position at TU Munich, she joined the IEO centre in 2003 and the School of Physics, DIT in 2008. Prof Naydenova's research group works on development of functionalised optical structures for application in sensing, security and micro-actuators. She is a Fellow of Optica and a member of SPIE. A full list of Prof Naydenova's research publications can be found here: https://orcid.org/0000-0002-0810-2197. e-mail: Izabela.naydenova@tudublin.ie